

## Article

# Thermal Degradation Studies of Poly(2-ethyl hexyl acrylate) in the Presence of Nematic Liquid Crystals

Amina Bouriche <sup>1,2</sup>, Lamia Alachaher-Bedjaoui <sup>1</sup>, Ana Barrera <sup>2</sup> , Jean-Noël Staelens <sup>2</sup>  and Ulrich Maschke <sup>2,\*</sup> 

<sup>1</sup> Laboratoire de Recherche sur les Macromolécules (LRM), Faculté des Sciences, Université AbouBekr Belkaid de Tlemcen (UABB), BP 119, Tlemcen 13000, Algeria

<sup>2</sup> Unité Matériaux et Transformations (UMET), UMR 8207, Université Lille, CNRS, INRAE, Centrale Lille, 59000 Lille, France

\* Correspondence: ulrich.maschke@univ-lille.fr; Tel.: +33-3-20-33-63-81

**Abstract:** The thermal degradation behavior of Poly(2-ethyl hexyl acrylate) (Poly(2-EHA)), blended with a commercially available nematic liquid crystal (LC) mixture, was investigated by thermal gravimetric analysis (TGA). Different heating rates, ranging from 5 to 200 °C/min, were applied under an inert atmosphere. Based on the TGA results, activation energies ( $E_{\alpha}$ ) at different conversion rates ( $\alpha$ ) were determined using three integral isoconversion methods: Flynn-Wall-Ozawa (FWO), Tang, and Kissinger-Akahira-Sunose (KAS). It can be noticed that the global evolution of these activation energies was the same for the three models. The coefficient of determination  $R^2$  presented values generally higher than 0.97. Using these models, the  $E_{\alpha}$  value for the LC remains constant at 64 kJ/mol for all conversions rates. For the polymer Poly(2-EHA), applying the Tang and FWO models, the activation energy presents a variation ranging from 80 kJ/mol, for conversion  $\alpha = 0.1$ , to 170 kJ/mol, for  $\alpha = 0.9$ . For the third model (KAS), this energy varies between 80 and 220 kJ/mol in the same range of  $\alpha$ .

**Keywords:** polymer; liquid crystal; thermal stability; thermogravimetric analysis; non-isothermal method



**Citation:** Bouriche, A.;

Alachaher-Bedjaoui, L.; Barrera, A.; Staelens, J.-N.; Maschke, U. Thermal Degradation Studies of Poly(2-ethyl hexyl acrylate) in the Presence of Nematic Liquid Crystals. *Polymers* **2023**, *15*, 3934. <https://doi.org/10.3390/polym15193934>

Academic Editor: Giulio Malucelli

Received: 28 July 2023

Revised: 20 September 2023

Accepted: 22 September 2023

Published: 29 September 2023



**Copyright:** © 2023 by the authors. Licensee MDPI, Basel, Switzerland. This article is an open access article distributed under the terms and conditions of the Creative Commons Attribution (CC BY) license (<https://creativecommons.org/licenses/by/4.0/>).

## 1. Introduction

Polymer dispersed liquid crystal (PDLC) films remain an important class of composite materials consisting of phase-separated micro-sized LC domains embedded in a continuous polymer matrix [1,2]. Recently, PDLC films have been widely investigated due to the electrically responsive and birefringent properties of LCs and the excellent properties of selected polymers such as good mechanical strength, flexibility and easy processability [3]. Inspired by the use of PDLC materials in display technologies, research on these materials has grown rapidly in the last decades and now extends beyond smart windows [4], displays [5], including diffuse [6], antipeeping and quantum dots (QDs) [7] devices, components of organic light-emitting diodes (OLEDs) [8], field-effect transistors (FETs) [9], energy storage [10] and solar energy harvesting [11].

Because polymeric materials are often used outdoors for long periods of time, they can be subject to degradation effects caused by heat, sunlight, atmospheric oxygen, moisture and stress. As a result, their chemical and physical properties deteriorate and the life of the material is limited. Therefore, any polymeric material to be used in outdoor applications must have excellent resistance to all environmental conditions. The thermal degradation behavior of polymers affects the final properties, such as the upper temperature limit of use and dimensional stability. The reliability of polymer materials can be improved and the competitiveness of a product increased by evaluating the durability and estimating the service life [12].

Few techniques are available to evaluate the durability of PDLC materials. Thermogravimetric analysis (TGA) is commonly used to determine the thermal decomposition

kinetics and thermal stability of polymers [13] and can be studied using single heating and multiple heating rate methods [14]. Model-free isoconversion methods [15,16] are the most reliable approaches for calculating activation energies of thermally activated reactions. A large number of isoconversion methods have been proposed, that allow the activation energy ( $E$ ) of a process to be estimated as a function of the degree of conversion ( $\alpha$ ) [17]. Analysis of the dependence of the activation energy on  $\alpha$  provides important clues about the degradation mechanism [18–22]. It is worth noting that when the activation energy is dependent on  $\alpha$  [23], the differential method proposed by Friedman [24] gives values of the activation energy that differ from those obtained by integral iso-conversion methods such as Flynn-Wall-Ozawa (FWO) [25,26], Li-Tang [27] and Kissinger-Akahira-Sunose (KAS) [28].

Thermal degradation reactions of polyacrylates generally occur through various re-action pathways leading to peroxides, alcohols, carbon dioxide, etc. along with depolymerized structures such as monomers [29–31]. In the presence of oxygen, the polymer degradation rate is usually higher than in an oxygen-free environment [32–34]. Hu et al. compared the thermal degradation of poly(butyl acrylate) (PBA) initiated by the combination of 3-caprolactam and thiols to initiate vinyl polymerization, and the novel system was found to be different from the traditional PBA initiated with azobisisobutyronitrile (AIBN). PBAs prepared with thiols have higher degradation temperatures and corresponding activation energies compared to those prepared with AIBN [35]. Indeed, PBA-thiols have an average activation energy of 170–212 kJ/mol, while that of PBA-AIBN was found to be 130 kJ/mol, using the KAS method. This energy varied between 155–182 kJ/mol for PBA-thiols and 113 kJ/mol for PBA-AIBN when the FWO method was used.

Qian et al. investigated different compositions of poly(2-ethylhexylacrylate/ $\alpha$ -methylstyrene) (2-EHA/MeSt) copolymers [36]. As the content of  $\alpha$ -MeSt units increased from 0 wt-% to 20 wt-%, the degradation activation energy of the copolymers increased from 127.1 to 148.5 kJ/mol. The FWO method showed that the value of the degradation activation energy of the  $\alpha$ -MeSt-20 sample was higher than that of  $\alpha$ -MeSt-0 at each conversion, and with the progress of the degradation reaction, the value of the degradation activation energy of  $\alpha$ -MeSt-20 gradually approached that of  $\alpha$ -MeSt-0. Ors and la Perrière [37] proposed a degradation mechanism of poly(isobornylacrylate) (poly(BOA)) leading to the formation of both camphene and a nortricyclic species. This two-step degradation mechanism was also observed by Matsumoto et al. [38]. A thermal degradation study of a polymer/LC system composed of poly(ethylene-co-methylacrylic acid) (PEMA) and 4-(3-hydroxypropoxy)-4'-cyanobiphenyl (H3CB) was carried out by Han et al. [39]. The temperature of maximum decomposition rate was observed to be 318 °C for H3CB and 492 °C for PEMA. The process of thermal decomposition under inert atmosphere involves chain scission effects, and interaction occurred between PEMA and H3CB. A two-step decomposition process occurred in nitrogen atmosphere.

Edina et al. studied the synthesis and characterization of nano-encapsulated LCs in a polymer (nanoELCP) obtained by soap-free emulsion polymerization of the system styrene (ST) and acrylic acid (AA) in the presence of the LC E7 [40]. TGA analyses were performed to quantify the amount of E7 encapsulated in the polymer particles [41]. The preparation and experimental studies of phase transitions and morphology of new PDLC systems based on Udel-3000 polysulfone (PSU) or its derivatives (chloromethylated PSU or PSU with a phosphaphenanthrene side substituent) and a phosphorus-containing LC polymer (LCP) were evaluated by Tachita et al. [42]. These researchers showed that the presence of the phosphorus atom in the structure of the LCP and also in the polymer matrix, based on phosphorylated PSU, improved the key properties such as flame retardancy, thermal stability, and so on.

Merah et al. synthesized Poly(BOA-co-2-EHA) copolymers via free radical photopolymerization/crosslinking reactions of BOA and 2-EHA, in the presence of 1,6-hexanedioldiacrylate (HDDA) as crosslinking agent, to obtain chemically crosslinked polymer networks [43]. Several degradation processes were observed by TGA, especially

that of the isobornylene group at low temperature, followed by the degradation of the carbon backbone at higher temperatures. Increasing IBOA content leads to a higher thermal stability of Poly (IBOA-co-2-EHA). The mass loss thermogram and its derivative of cross-linked poly(2-EHA) revealed that its thermal degradation takes place in a single step between 593 and 693 K, corresponding to the decomposition of the carbon skeleton. This observation has already been made by Haloi and Singha [44], by investigating the thermal degradation of poly(2-EHA)/nanocomposite clay in an interval from 597 and 687 K.

Although much research has been done on thermal effects related to physical properties of polymers, not many studies are known to have investigated the kinetics of thermal decomposition and thermal stability of polymer/LC blends. In the present work, a model polymer/LC system was investigated by TGA using different heating rates. The system investigated here is composed of linear poly(2-EHA) and the eutectic nematic blend E7, by varying their composition. Three multiple heating rate methods, Li Tang, FWO and KAS, were applied to calculate the activation energies of thermal decomposition. The local linear integral isoconversion method (LL-INT) was chosen to evaluate the activation energy dependencies under non-isothermal conditions [45].

## 2. Materials and Methods

### 2.1. Materials

Poly(2-EHA) (see Figure 1a) was supplied by Sigma Aldrich (Saint Quentin Fallavier, France). Its molecular weight and polydispersity ( $M_w/M_n$ ) were determined by gel permeation chromatography (GPC), yielding  $M_w = 92.000$  g/mol and  $M_w/M_n = 3$ .

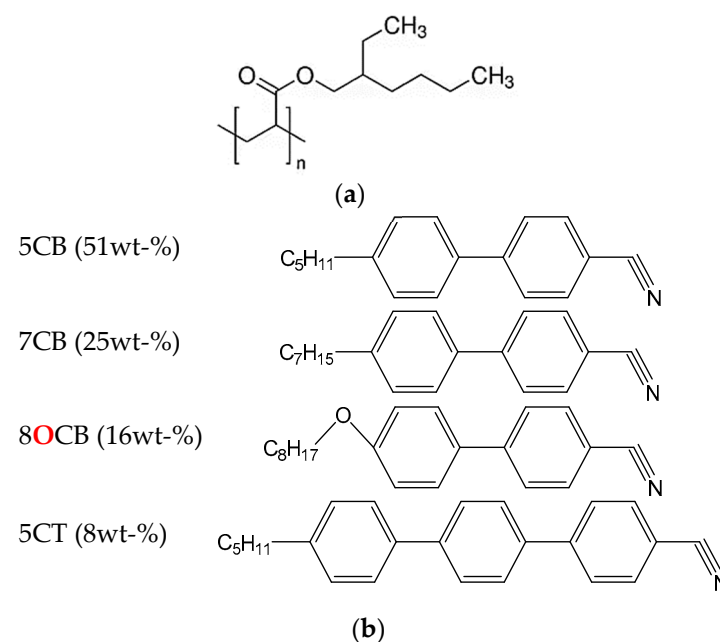


**Figure 1.** Chemical structures of (a) Poly 2-EHA and (b) E7.

E7 represents a well-known nematic LC mixture (see Figure 1b), commercially available from Synthon GmbH (Wolfen, Germany). This eutectic mixture contains 51 wt-% of 4-cyano-4'-n-pentyl-biphenyl (5CB), 25 wt-% of 4-cyano-4'-n-heptyl-biphenyl (7CB), 16 wt-% of 4-cyano-4'-n-oxyoctyl-biphenyl (8OCB) and 8 wt-% of 4-cyano-4'-n-pentyl-p-biphenyl (5CT) [46]. E7 exhibits a single nematic-isotropic transition temperature ( $T_{NI}$ ) at +61 °C, and a glass transition temperature ( $T_g$ ) at −61 °C [47]. The ordinary ( $n_o$ ) and extraordinary ( $n_e$ ) refractive indices of E7 at  $T = 20$  °C are given as  $n_o = 1.5183$ ;  $n_e = 1.7378$  ( $\lambda = 632.8$  nm), leading to an optical birefringence of  $\Delta n = n_e - n_o = 0.2195$  [48]. The chemical structures of the components of E7 used in this study are shown in Figure 1b). The poly 2-EHA/E7 blends were prepared by a thermally induced phase separation process.  $x$  wt-% of E7 ( $x = 10$ ,

20, . . . , 90) and  $(100 - x)$  wt-% of poly-2EHA were mixed together at room temperature for several hours. Detailed data on the evolution of the glass transition and the transition from the nematic + isotropic to the isotropic states of the poly-2-EHA/E7 mixtures with composition are given in reference [47]. Some optical data are also given [47].

## 2.2. Thermogravimetric Analysis

TGA was performed on a Perkin Elmer Pyris 1 analyzer (Perkin Elmer, Waltham, MA, USA) with a mass resolution of 1  $\mu\text{g}$  using HT platinum plates. Analysis of samples with an average weight of 8 mg was performed under a nitrogen atmosphere at a flow rate of 20 mL/min. The precise temperature was measured by a thermocouple in direct contact with the sample crucible. Thermogravimetric analysis of the polymer/LC samples was performed in dynamic mode using constant masses subjected to a series of heating rates  $\beta$  (5, 10, 20, 50, 100 and 200  $^{\circ}\text{C}/\text{min}$ ), applying a temperature interval between 20  $^{\circ}\text{C}$  and 800  $^{\circ}\text{C}$ .

## 2.3. Gel permeation Chromatography

Gel permeation chromatography (GPC) analysis was performed at room temperature on a Waters Alliance e2695 system (Waters S.A.S., Saint-Quentin en Yvelines, France) using differential refractive index (Wyatt RI) and multi-angle light scattering (Wyatt MALS,  $\lambda$  (laser) = 670 nm) detectors. Three columns were coupled in series (Styragel HR1, Styragel HR3, Styragel HR4). Tetrahydrofuran (THF) was used as solvent (flow rate 1 mL/min) and calibration was performed with polystyrene (PS) standards from Polymer Laboratories. A fixed amount of 5 mg of the sample was dissolved in 5 mL of THF and filtered through a 0.20  $\mu\text{m}$  filter to remove undissolved particles.

## 2.4. Polarized Optical Microscopy

Polarized Optical Microscopy (POM) experiments were performed using an Olympus BX41 equipped with a Linkam LTS350 heating/cooling stage and a TMS 94 temperature control unit. Specimens were placed between two microscope slides, heated until optically clear, and then slowly cooled to ambient temperature. The heating and cooling rates were 0.5  $^{\circ}\text{C}/\text{min}$ . The same heating and cooling procedures were repeated three times for each sample to minimize experimental uncertainty.

## 3. Kinetic Study of Degradation

In thermogravimetric measurements, the degree of decomposition (conversion) can be calculated as follows

$$\alpha = \frac{m_0 - m_t}{m_0 - m_f} \quad (1)$$

where  $\alpha$  represents the relative decomposition conversion [49].  $m_0$ ,  $m_f$ , and  $m_t$  correspond to the masses of the sample ( $m_0$ , in the initial state;  $m_f$ , in the final state,  $m_t$ , at any given time  $t$ ).  $\alpha$  was set to 0 and 1 for the initial and final measurement data, respectively [49].

A typical model for a kinetic process can be represented as follows

$$d\alpha/dt = k f(\alpha) \quad (2)$$

where  $d\alpha/dt$  stands for the decomposition rate,  $k$  is a decomposition rate constant that can be expressed as  $\alpha$ , and  $f(\alpha)$  represents the function of  $\alpha$  which depends on the decomposition mechanism. The relationship between reaction rate and extent of reaction can be generally expressed in the form

$$d\alpha/dt = A \exp(-E_\alpha/RT) f(\alpha) \quad (3)$$

where  $A$  is the pre-exponential factor ( $\text{s}^{-1}$ ),  $E_\alpha$  stands for the activation energy (J/mol),  $R$  represents the gas constant (8.314 J/mol K), and  $T$  corresponds to the temperature in Kelvin [50].

### 3.1. Tang Method

This method represents an integral method, using an approximation of the integral temperature as proposed by Tang et al. [51]

$$\ln\left(\frac{\beta}{T_{\alpha}^{1.894661}}\right) = C_T(\alpha) - 1.0014\left(\frac{E_{\alpha}}{RT_{\alpha i}}\right) \quad (4)$$

where  $C_T(\alpha)$  is a constant equal to  $\left[\ln\frac{AE_{\alpha}}{g(\alpha)R} + 3.6350 - 1.8946nE_{\alpha}\right]$ . The index  $i$  denotes different heating rates. For each degree of conversion  $\alpha$ , a corresponding  $T_{\alpha i}$  and a heating rate are used.  $E_{\alpha}$  is evaluated from the slope of the linear regression of the plot  $\ln\left(\frac{\beta}{T_{\alpha i}^{1.894661}}\right)$  as a function of  $1/T$  [52].

### 3.2. Flynn-Wall-Ozawa Method

The FWO method is a model-free method developed by Flynn and Wall [53] as well as by Ozawa. FWO uses Doyle's [54] equation for the approximation of the temperature integral. Considering the approximation  $\ln p(x) = -5.331 - 1.052x$ , Equation (3) can be converted into

$$\ln\beta = C_W(\alpha) - 1.052\frac{E_{\alpha}}{RT_{\alpha i}} \quad (5)$$

where  $C_W(\alpha)$  stands for a constant equal to  $\ln\left[\frac{AE_{\alpha}}{g(\alpha)R}\right] - 5.331$ .  $E_{\alpha}$  is evaluated from the slope of the linear regression of the plot  $\ln\beta$  as a function of  $1/T_{\alpha i}$  [55].

### 3.3. Kissinger-Akahira-Sunose Method

The method of KAS is also known as the generalized Kissinger method [56]. This isoconversional integral method, based on the Murray and White approximation, is given by

$$\ln\frac{\beta_i}{T_{\alpha i}^2} = C_K(\alpha) - \frac{E_{\alpha}}{RT_{\alpha i}} \quad (6)$$

where  $C_K(\alpha)$  represents a constant equal to  $\ln\frac{AR}{E_{\alpha}g(\alpha)}$ .  $E_{\alpha}$  can be calculated from the slope obtained by plotting  $\ln\frac{\beta_i}{T_{\alpha i}^2}$  as function of  $1/T_{\alpha i}$  [57].

## 4. Results and Discussion

Thermogravimetric curves and their derivatives (DTG) have been used to evaluate the thermal stability of poly(2-EHA)/E7 blends. The area of the DTG peak is directly proportional to the mass loss of the material over the same temperature range, and the height of the (DTG) peak indicates the rate of mass loss at the corresponding temperature.

### 4.1. Liquid Crystal E7

The evolution of the mass loss (in %) and the rate of mass loss (DTA) during the decomposition of E7, obtained by applying different heating rates, are shown in Figures 2a and 2b, respectively. This LC mixture remains thermally stable up to 180 °C at a heating rate of 5 °C/min. Total degradation was achieved around 300 °C. On the other hand, when a heating rate of 200 °C/min is applied, the range of thermal stability is extended up to 310 °C, and total degradation occurs at 450 °C. It can be concluded that the temperature corresponding to the maximum of the mass derivative increases with the heating rate, together with the expansion of the temperature range of thermal stability.

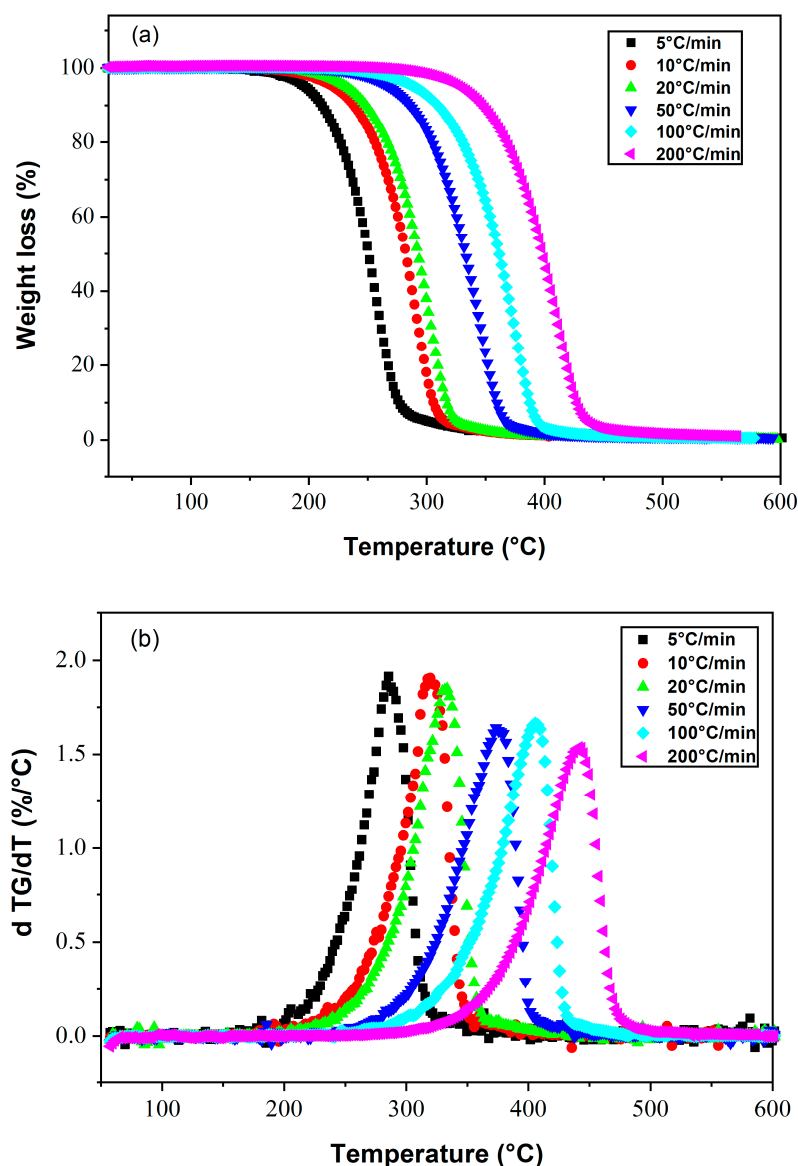


**Figure 2.** Thermograms presenting (a) the weight losses and (b) their derivatives as a function of temperature for the LC E7, at different heating rates.

#### 4.2. Poly(2-Ethylhexylacrylate)

Thermal degradation of polyacrylates in air occurs by peroxide formation, radical reactions with oxygen leading to depolymerization, formation of alcohols, carbon dioxide, etc. In the absence of oxygen, polyacrylates degrade by rearrangements leading to decarboxylation and formation of monomers and alcohols [58]. Figure 3a shows the degradation kinetics of poly(2-EHA) at different heating rates, and Figure 3b shows the derivatives of mass loss as a function of temperature. A thermal stabilization was observed between 25 °C and 250 °C for the lowest heating rate (5 °C/min), which broadened as the heating rate increased. The degradation temperature of poly(2-EHA) was determined at the peak maximum as shown in Figure 3b. The appearance of two shoulders was noticed, the first appeared in the temperature range from 150 to 370 °C and the second in the interval from 400 to 450 °C. The latter disappeared by increasing the heating rate. This phenomenon can be related to the mobility of the chain segments of the linear poly(2-EHA) and was not observed in the case of crosslinked polymers, where the zone of thermal stability increases with the increase of the crosslinking rate [59].

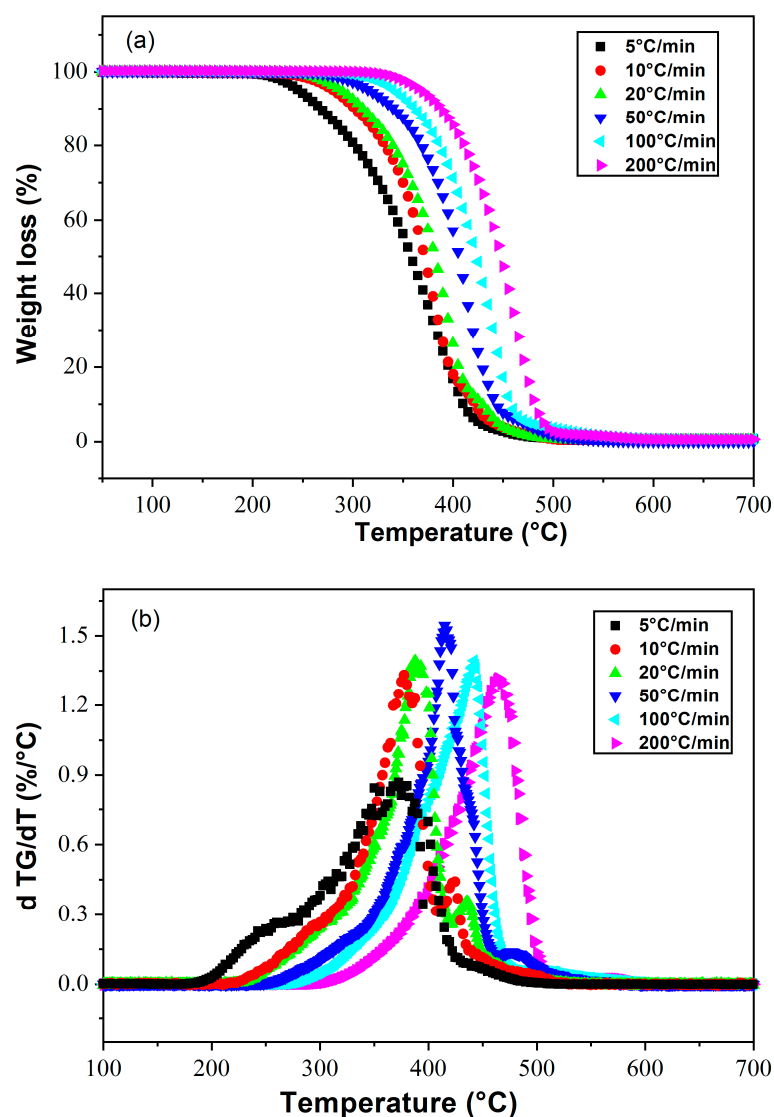


**Figure 3.** Thermograms presenting (a) the weight losses and (b) their derivatives as a function of temperature for Poly(2-EHA), at different heating rates.

A qualitative review of the thermal degradation reactions occurring on linear poly(2-EHA) has been performed by Grassie et al. [60]. In particular, the thermal volatilization analysis of poly(2-EHA) leads to a two-step degradation mechanism (see Figure 6 of [60]). The molecular origin of such double degradation phenomena has been described by Aliev et al. [61] who studied the thermal stability of poly(alkyl acrylates). In fact, the degradation proceeds in two stages, corresponding to two mechanisms of polymer depolymerization with random chain initiation at the ends of the molecule and inside the molecule.

#### 4.3. Poly(2-EHA)/E7 Blends

Figure 4 shows the loss of mass (Figure 4a) and its derivatives (Figure 4b) as a function of temperature of Poly(2-EHA)/E7 mixtures for different sample compositions, for a heating rate of 10 °C/min. For blends containing high concentrations of E7 (above 60 wt-%), the TGA results showed a thermal behavior similar to that of pure E7. In this case, a single degradation temperature corresponding to E7 was observed, which increased with the concentration of LC. For lower E7 content (below 60 wt-%), two degradation temperatures were observed, one corresponding to Poly(2-EHA), and the other to the LC. For polymer-rich mixtures, a slight variation in the degradation temperatures of E7 and polymer was observed.

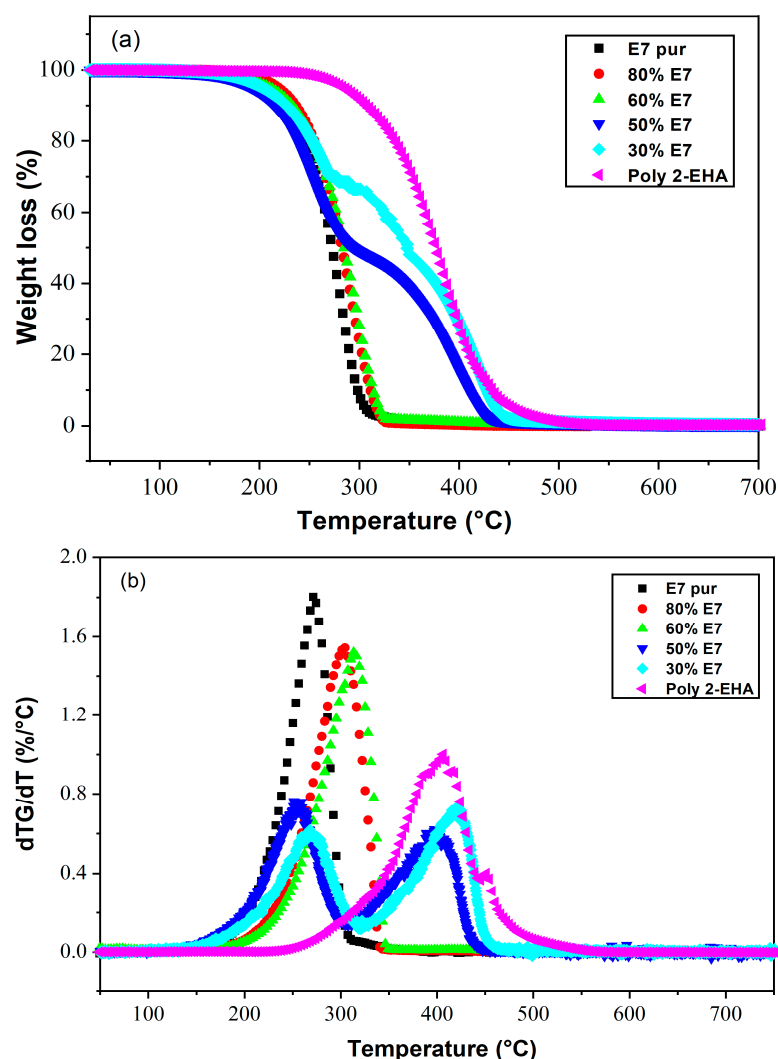


**Figure 4.** Thermograms presenting (a) the weight losses and (b) their derivatives as functions of temperature and composition for Poly(2-EHA)/E7 mixtures (heating rate: 10 °C/min).

These observations can be explained by the evolution of the phase behavior, i.e., the morphologies, as a function of sample composition. As will be shown in the next Section 4.4, at higher E7 concentrations (above 60 wt-% E7) coalescence phenomena occur, resulting in large LC droplets that dominate the sample morphology, so that only a single degradation temperature was observed. On the other hand, as shown in Figure 4, at lower E7 concentrations (below 60 wt-% E7), separated small LC domains are present, resulting in the appearance of two degradation temperatures.

The results obtained by TGA were rationalized by isoconversion methods to calculate the kinetic parameters. In particular,  $E_{\alpha}$  was obtained using theoretical methods developed by Tang, FWO and KAS.

#### 4.4. Observation of Sample Morphology of Poly(2-EHA)/E7 Blends

Analysis of the morphology of p-2EHA/E7 mixtures with POM makes it possible to observe the variation of the texture of the LCs as a function of temperature and sample composition. Figure 5 shows some POM images of such sample morphologies of these mixtures with different concentrations of E7, taken at 58 °C with crossed polarizer/analyzer. This temperature is close to the nematic-isotropic transition temperature. For mixtures with low E7 content (30 wt-% and 40 wt-%, Figure 5a,b), the LC was already phase-separated from the polymer and presented small but distinguishable droplets. The droplets decrease in number and increase in size for blends above 40 wt-% E7 (Figure 5c–f). Coalescence

phenomena of the LC droplets occur and are clearly visible on the POM scale, especially for mixtures above 70 wt-% E7 (Figure 5d). At 80 and 90 wt-% E7 (Figure 5e,f), coalescence effects lead to large scale patterns with dimensions of several hundreds of  $\mu\text{m}$ .

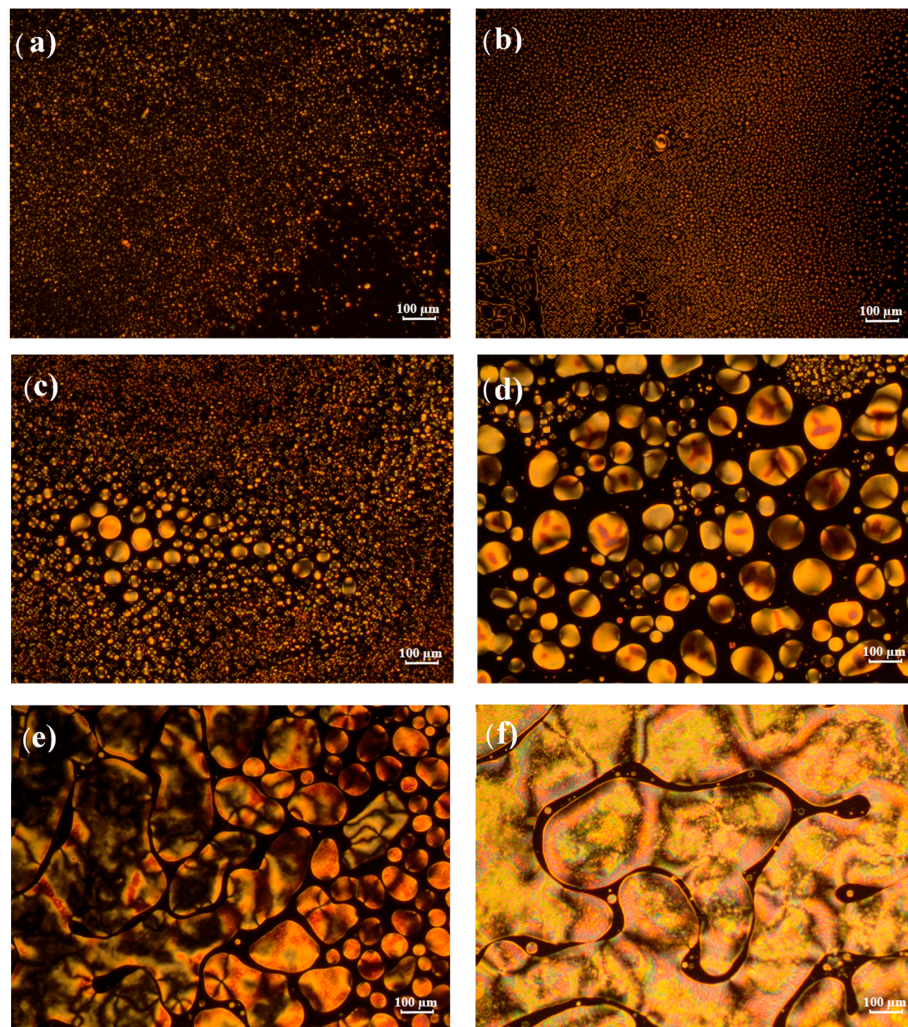


**Figure 5.** Texture of Poly-2 EHA/E7 samples at different concentrations observed at 58 °C in the nematic + isotropic state: (a) 30 wt-% E7, (b) 40 wt-% E7, (c) 60 wt-% E7, (d) 70 wt-% E7, (e) 80 wt-% E7, and (f) 90 wt-% E7.

#### 4.5. Determination of Activation Energy

The determination of the activation energy allows to estimate the number of steps involved in a reaction and the nature of the processes involved [62]. The variation of the activation energy as a function of the degree of conversion  $\alpha$  was studied using the iso-conversion methods presented in Section 3. The kinetic parameters obtained by the methods of Tang, FWO and KAS were calculated according to Equation (5), (6) and (7), respectively, for values of conversion  $\alpha$  from 0.1 to 0.9. To determine the kinetic parameters, the same value of  $\alpha$  was chosen for all curves with different heating rates. Figure 6 shows a representation of  $\ln\left(\frac{\beta}{T_{ai}^{1.89466T}}\right)$  versus  $1/T$ , according to the Tang method, for different conversion values. The corresponding results from the FWO approach are shown in Figure 7, where  $\ln\beta$  is given as a function of  $1/T$ . Finally, Figure 8 shows plots of  $\ln\frac{\beta_i}{T_{ai}^2}$  as a function of  $1/T$ , corresponding to the KAS method. The curves obtained by these three methods represent a linear behavior for all compositions studied, applying different heating rates. The  $E_\alpha$  values were calculated from the slopes of these lines.

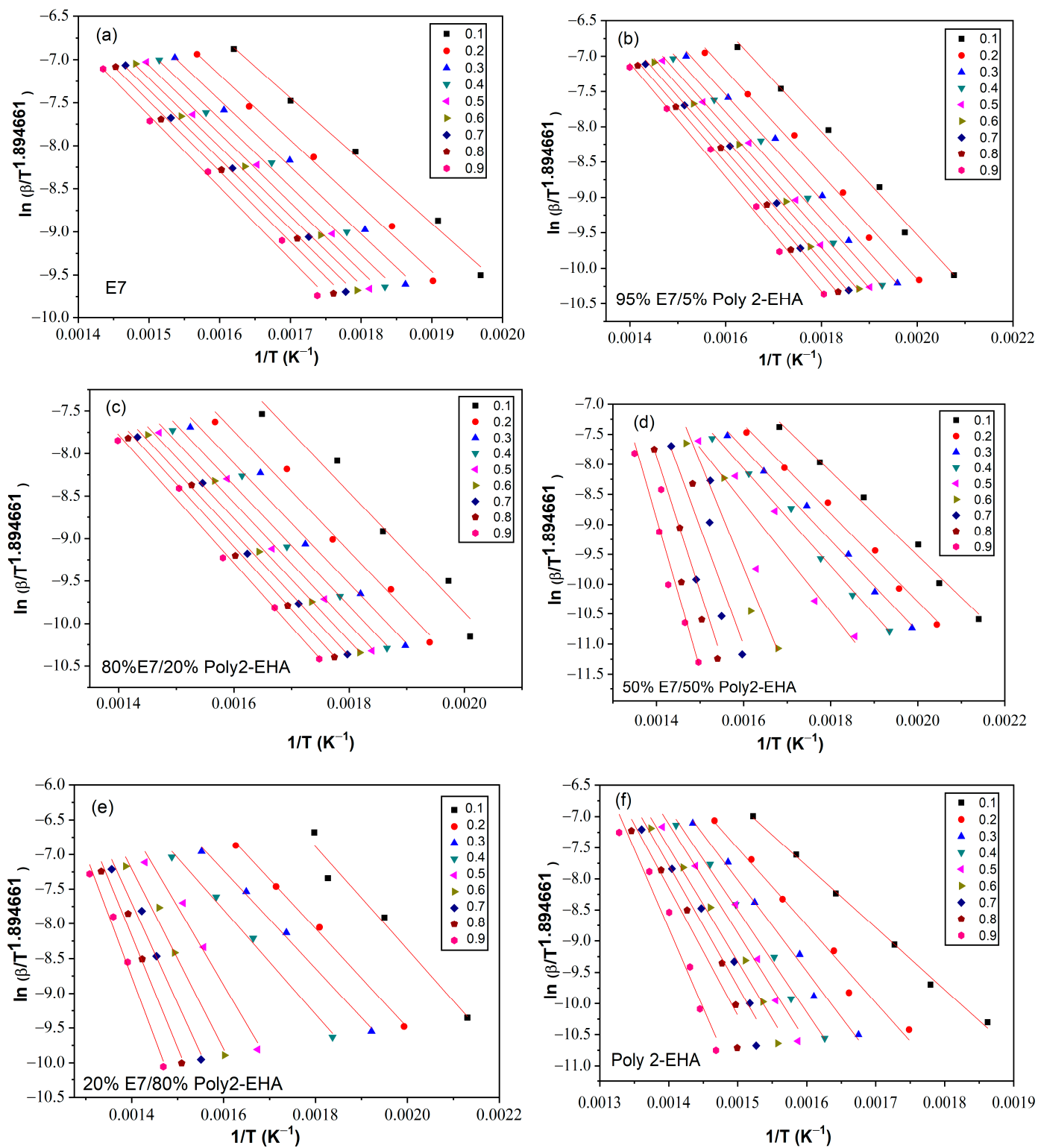


**Figure 6.**  $\ln(\beta/T^{1.894661})$  as function of  $1/T$  for Poly(2-EHA)/E7 mixtures, according to the conversion  $\alpha$ , using the approach of Tang et al. (a) 100 wt-% E7, (b) 95 wt-% E7, (c) 80 wt-% E7, (d) 50 wt-% E7, (e) 20 wt-% E7 and (f) Poly(2-EHA).

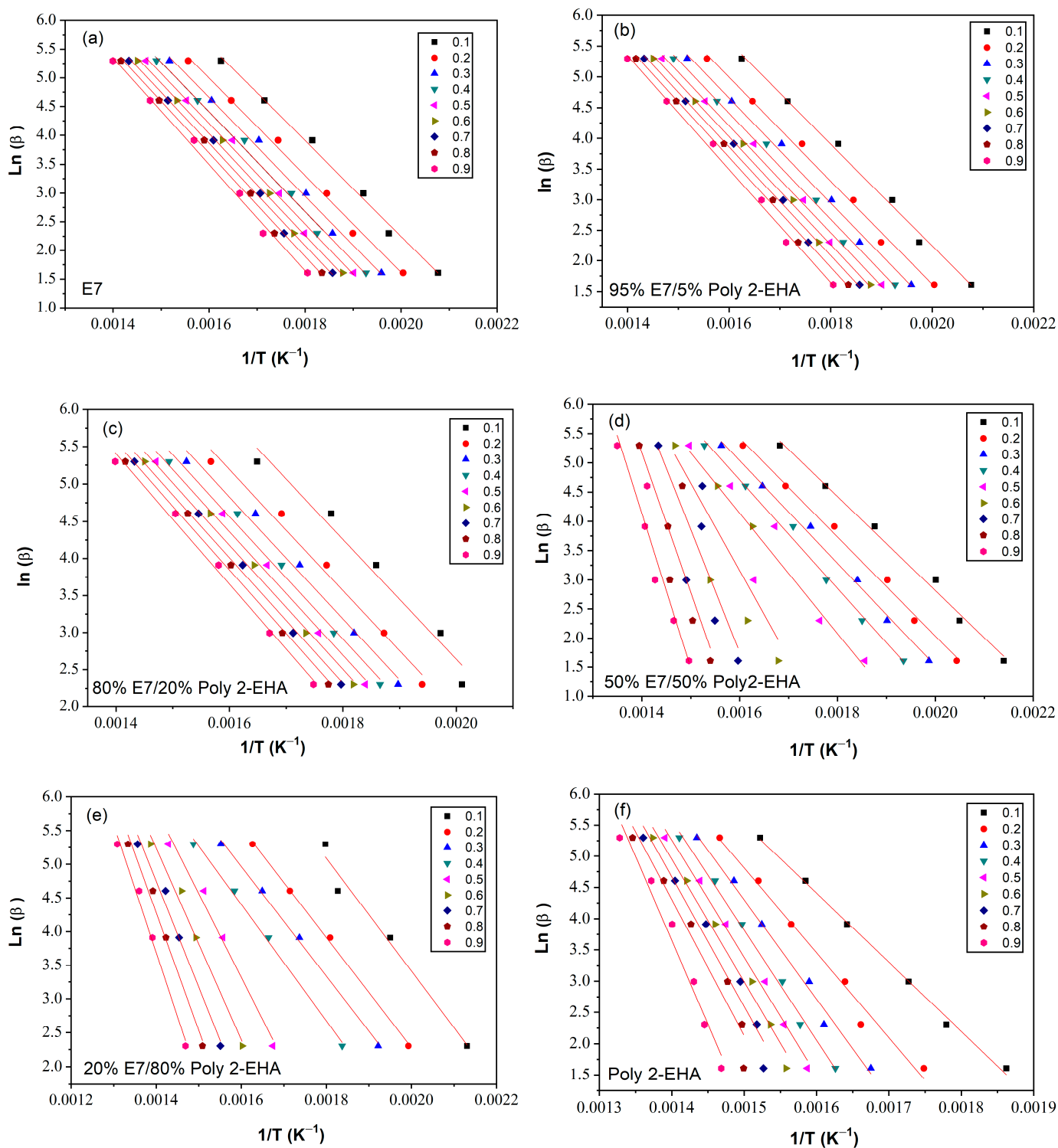


**Figure 7.**  $\ln(\beta)$  as function of  $1/T$  for Poly(2-EHA)/E7 mixtures, according to the conversion  $\alpha$ , applying the approach of FWO et al. (a) 100 wt-% E7, (b) 95 wt-% E7, (c) 80 wt-% E7, (d) 50 wt-% E7, (e) 20 wt-% E7 and (f) Poly(2-EHA).

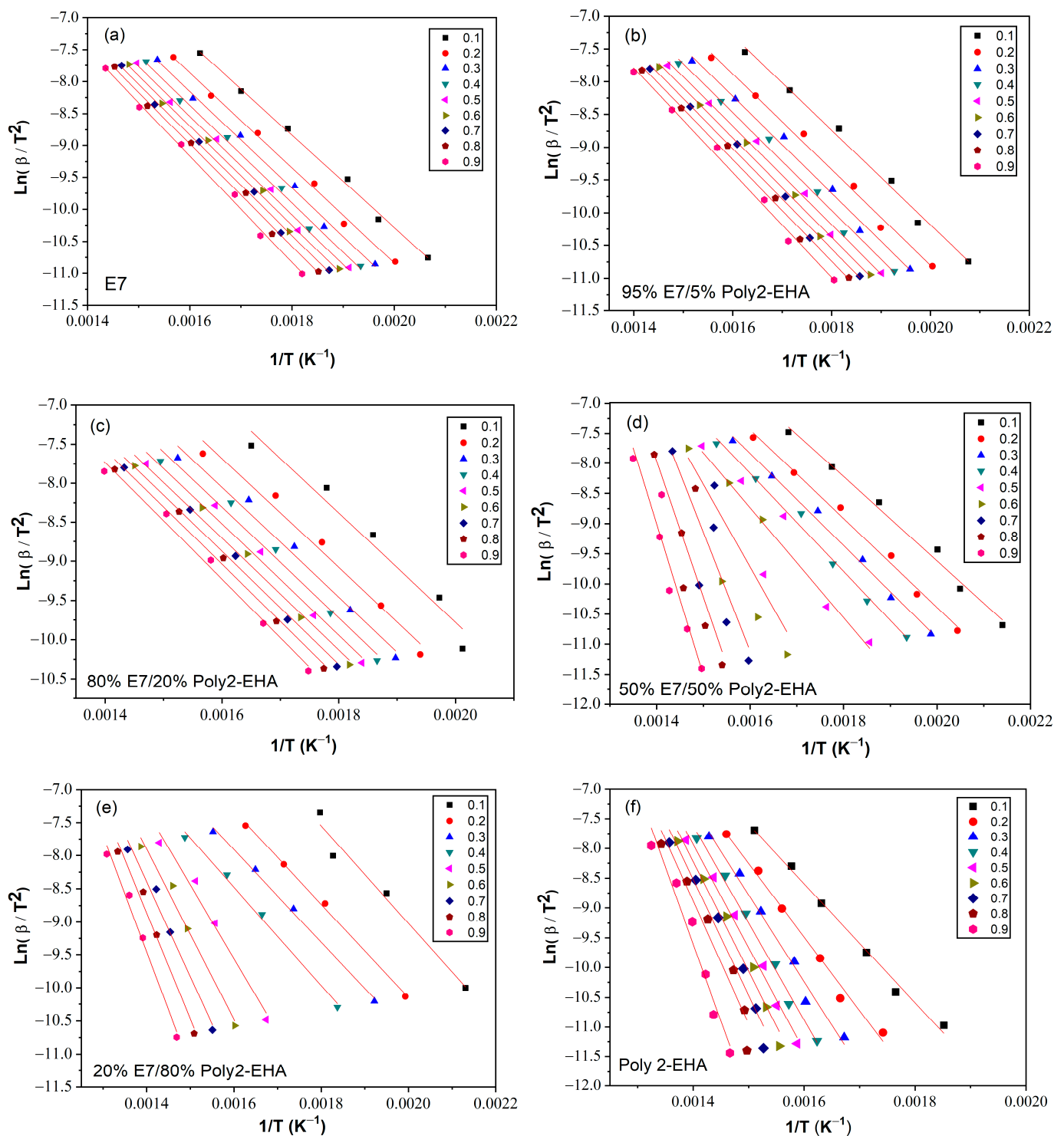


**Figure 8.**  $\text{Ln}(\beta/T^2)$  as function of  $1/T$  for Poly(2-EHA)/E7 mixtures, according to the conversion  $\alpha$ , using the approach of KAS et al. [63]. (a) 100 wt-% E7, (b) 95 wt-% E7, (c) 80 wt-% E7, (d) 50 wt-% E7, (e) 20 wt-% E7 and (f) Poly(2-EHA).

Table 1 summarizes the results of the thermal activation energies calculated from the three theoretical models for the poly(2-EHA)/E7 system. It can be seen that the global evolution of these activation energies was the same for the three models. The coefficient of determination  $R^2$  presented values generally higher than 0.97. However, the 50 wt-% mixture presented lower  $R^2$  data because two degradation processes were observed, that of the LC and that of the poly(2-EHA).

**Table 1.** Activation energies and regression parameters  $R^2$  for Poly(2-EHA)/E7 mixtures.  $R^2$  represents a goodness-of-fit measure for linear regression.

Composition	Conversion	Tang Model		FWO Model		Kissinger Model	
		$E_a$ (kJ/mol)	$R^2$	$E_a$ (kJ/mol)	$R^2$	$E_a$ (kJ/mol)	$R^2$
E7	0.1	60.52	0.9933	65.69	0.9964	60.01	0.9962
	0.2	63.15	0.9927	67.66	0.9960	61.78	0.9955
	0.3	64.46	0.9918	68.86	0.9958	62.85	0.9948
	0.4	65.46	0.9899	69.80	0.9951	63.70	0.9936
	0.5	66.13	0.9900	70.49	0.9951	64.30	0.9936
	0.6	66.43	0.9895	71.06	0.9951	64.80	0.9935
	0.7	66.93	0.9907	71.86	0.9960	65.55	0.9945
	0.8	67.69	0.9907	73.01	0.9966	66.66	0.9947
	0.9	69.19	0.9912	75.56	0.9973	69.19	0.9950
95% E7	0.1	60.48	0.9905	65.74	0.9931	60.10	0.9903
	0.2	61.18	0.9906	66.73	0.9931	60.77	0.9904
	0.3	61.85	0.9906	67.57	0.9932	61.43	0.9905
	0.4	62.48	0.9903	68.32	0.9930	62.05	0.9901
	0.5	63.00	0.9903	68.94	0.9929	62.57	0.9901
	0.6	63.65	0.9905	69.67	0.9930	63.21	0.9903
	0.7	64.07	0.9899	70.18	0.9927	63.63	0.9898
	0.8	64.88	0.9906	71.06	0.9932	64.43	0.9904
	0.9	66.89	0.9909	73.10	0.9934	66.43	0.9907
80%E7	0.1	58.4	0.9484	63.93	0.9618	58.17	0.9857
	0.2	58.47	0.9736	64.25	0.9814	58.05	0.9847
	0.3	58.85	0.9784	64.83	0.9850	58.42	0.9827
	0.4	59.55	0.9786	65.28	0.9851	58.85	0.9817
	0.5	59.76	0.9800	65.79	0.9862	59.11	0.9796
	0.6	60.37	0.9821	66.10	0.9877	59.30	0.9783
	0.7	61.26	0.9831	66.80	0.9884	59.91	0.9779
	0.8	62.62	0.9850	67.76	0.9898	60.80	0.9731
	0.9	63.85	0.9860	69.19	0.9905	62.16	0.9512
50% E7	0.1	58.27	0.9873	63.66	0.9910	58.20	0.8892
	0.2	61.37	0.9907	66.99	0.9935	61.29	0.6081
	0.3	63.66	0.9924	69.42	0.9947	63.58	0.5532
	0.4	67.64	0.9883	73.42	0.9917	67.56	0.4926
	0.5	75.80	0.8292	81.45	0.8617	75.72	0.8289
	0.6	146.88	0.8643	118.28	0.5453	113.84	0.9887
	0.7	163.73	0.5535	166.07	0.5900	163.65	0.9924
	0.8	187.37	0.6083	188.88	0.6391	187.29	0.9906
	0.9	208.59	0.8893	209.38	0.8998	208.50	0.9873
20% E7	0.1	61.54	0.9582	66.24	0.9671	61.19	0.9815
	0.2	59.14	0.9964	64.60	0.9977	58.74	0.9771
	0.3	58.62	0.995	64.44	0.9968	58.20	0.9758
	0.4	62.30	0.9921	68.34	0.9948	61.86	0.9749
	0.5	93.29	0.9724	98.49	0.9783	92.86	0.9720
	0.6	107.54	0.9752	112.43	0.9799	107.11	0.9919
	0.7	119.80	0.9761	124.39	0.9803	119.37	0.9948
	0.8	133.95	0.9774	138.09	0.9811	133.53	0.9963
	0.9	146.45	0.9816	150.24	0.9845	146.03	0.9577
Poly(2-EHA)	0.1	82.50	0.9959	91.95	0.9964	82.97	0.9857
	0.2	102.87	0.9788	112.86	0.9819	102.64	0.9847
	0.3	121.60	0.9865	131.94	0.9884	121.27	0.9827
	0.4	135.64	0.9921	146.23	0.9932	135.56	0.9817
	0.5	145.50	0.9608	156.38	0.9909	144.12	0.9796
	0.6	151.96	0.7164	162.93	0.9799	153.05	0.9783
	0.7	161.41	0.9476	172.55	0.9541	171.74	0.9779
	0.8	165.16	0.9825	180.93	0.9359	191.21	0.9731
	0.9	170.64	0.9598	223.22	0.9640	214.99	0.9512

Figure 9a, b and c shows the plots of  $E_\alpha$  of the Poly 2-EHA/E7 mixtures as a function of conversion  $\alpha$ , determined by the Tang, FWO and KAS methods, respectively. The  $E_\alpha$  value for the LC E7 remains constant at 64 kJ/mol for all conversions  $\alpha$ , for the three models. For the polymer Poly(2-EHA), using Tang and FWO models, the activation energy shows a variation ranging from 80 kJ/mol, for conversion  $\alpha = 0.1$ , to 170 kJ/mol for  $\alpha = 0.9$ . For the third model (KAS), this energy varies between 80 and 220 kJ/mol in the same range of  $\alpha$ . In the case of photochemically crosslinked Poly(2-EHA), Merah et al. [43] observed a single degradation step, characterized by an activation energy estimated at 293 kJ/mol. This energy corresponds to the entire thermal decomposition of Poly(2-EHA), which mainly produces monomers through a so-called unzipping process. For LC-rich mixtures, the activation energy remains constant with the conversion so that the obtained values were practically identical to those of pure LC. In these blends (above 50 wt-% E7), the LCs phase separate to form macroscopic domains and thus determine the total activation energy. In the case of polymer-rich mixtures, the activation energy remains constant over the conversion interval from 0.1 to 0.6. Beyond  $\alpha = 0.6$ , using the method of Tang et al., it increases to values between 140 and 160 kJ/mol. These values change slightly using the other two methods:

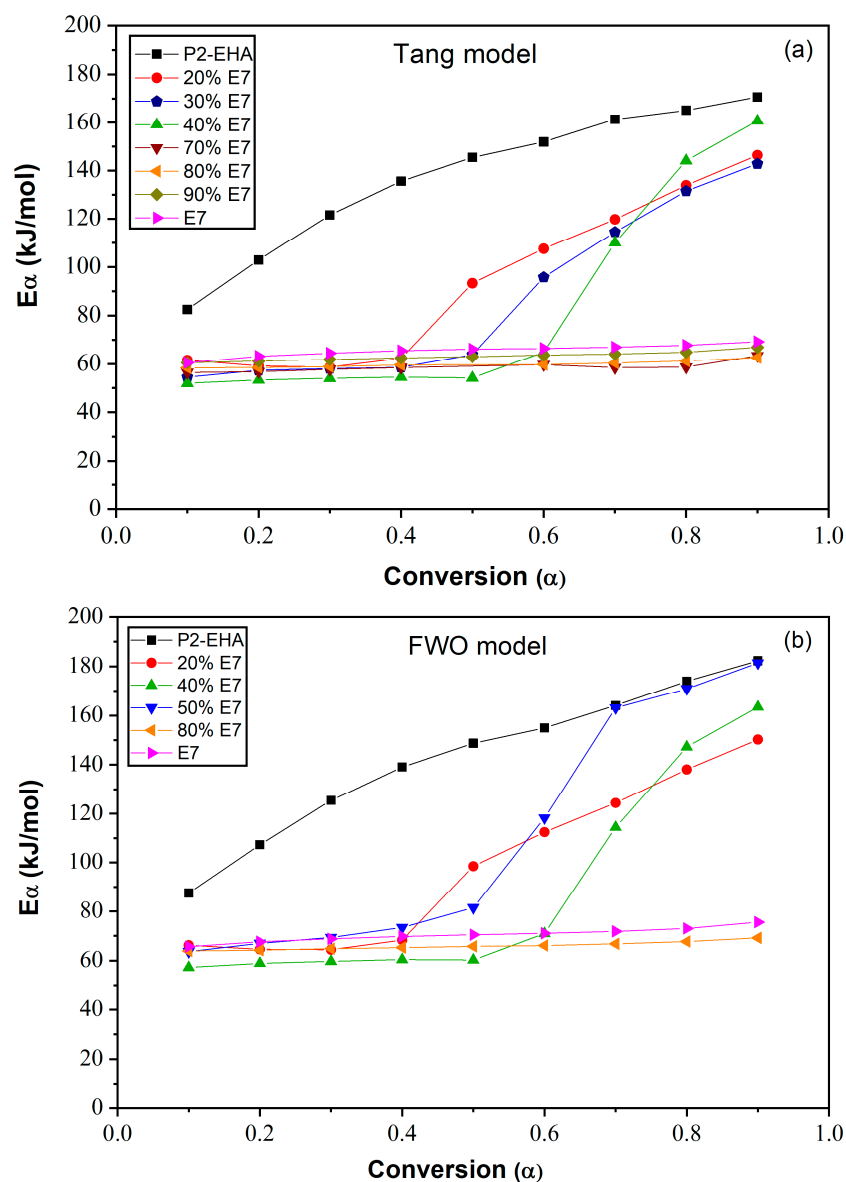
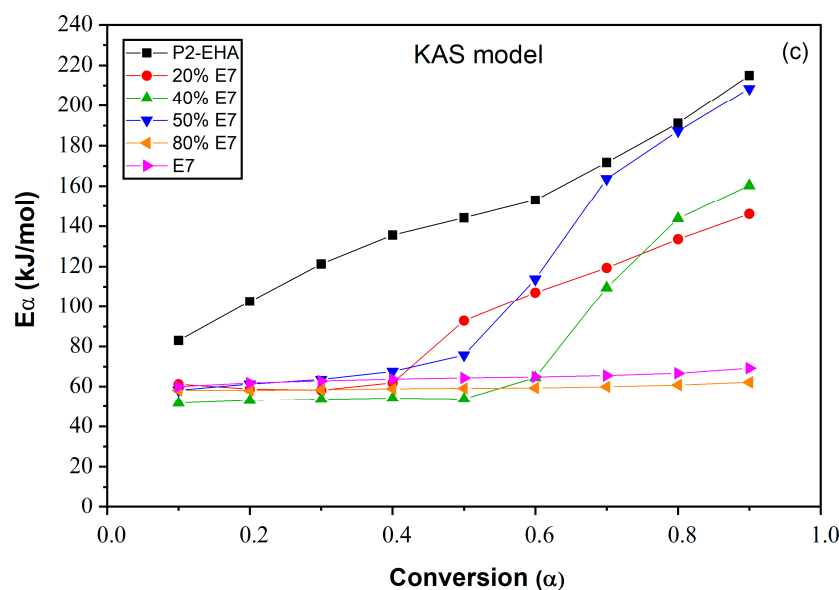


Figure 9. Cont.



**Figure 9.** Variation of the apparent activation energies of E7 and Poly(2-EHA) and their mixtures according to the conversion  $\alpha$ : (a) Tang model, (b) FWO model and (c) KAS model.

In the case of the FWO model,  $E_\alpha$  varies between 80 and 180 kJ/mol, while for the KAS method, values between 80 and 200 kJ/mol were obtained.

Figure 10 shows the dependence of  $E_\alpha$  on  $\alpha$  for the LC E7. The activation energy increases with the degree of conversion regardless of the isoconversion method used. The  $E_\alpha$  values obtained from the Tang method were found to be close to those collected from the KAS method, varying between 60 kJ/mol and 69 kJ/mol. For the FWO model, this energy increases from 65 kJ/mol to 75 kJ/mol with increasing  $\alpha$ . For a given value of  $\alpha$ ,  $E_{FWO} > E_{Tang} \approx E_{KAS}$ .

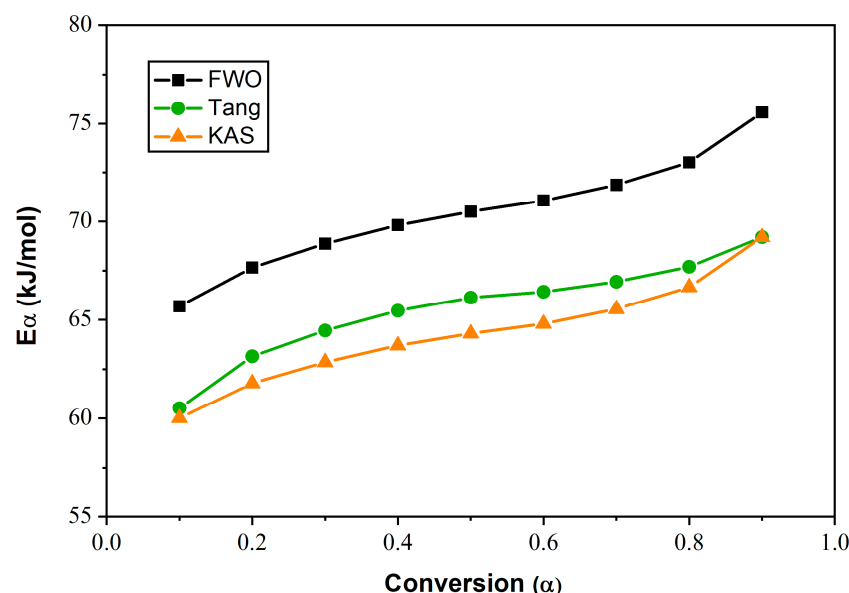


**Figure 10.** Dependence of  $E_\alpha$  on conversion  $\alpha$  for E7, evaluated by Tang, FWO and KAS methods.

## 5. Conclusions

The thermal degradation kinetics and stability of a model polymer/LC system were investigated by TGA. The system investigated in this report consists of linear poly(2-EHA) and the eutectic nematic LC mixture E7. Different heating rates were used for TGA under nitrogen atmosphere. For poly(2-EHA)/E7 blends containing high concentrations of E7,

the TGA results showed a thermal behavior similar to that of pure E7. In this case, a single degradation temperature corresponding to E7 was observed, which increases with the concentration of LC. For lower E7 content, two degradation temperatures were observed, one corresponding to poly(2-EHA) and the other to LC. For polymer-rich mixtures, a slight variation in the degradation temperatures of E7 and polymer was observed.

The results obtained by TGA were rationalized by isoconversion methods to derive kinetic parameters. In particular,  $E_a$  was calculated at different conversion rates ( $\alpha$ ), using theoretical methods developed by Tang, FWO and KAS. Good agreement between all the theories and experimental data was obtained. The coefficient of determination  $R^2$  of the linear relationships presented values generally higher than 0.97.

**Author Contributions:** Conceptualization, L.A.-B. and U.M.; methodology, A.B. (Amina Bouriche), L.A.-B. and U.M.; investigation, A.B. (Amina Bouriche), A.B. (Ana Barrera) and J.-N.S.; writing—original draft preparation, A.B. (Amina Bouriche); writing—review and editing, U.M.; supervision, L.A.-B. and U.M. All authors have read and agreed to the published version of the manuscript.

**Funding:** The APC was funded by the University of Lille/France.

**Institutional Review Board Statement:** Not applicable.

**Informed Consent Statement:** Not applicable.

**Data Availability Statement:** Data set presented in this study is available in this article.

**Acknowledgments:** This work is the result of a close collaboration between the two laboratories LRM of the UABB and UMET of the University of Lille, within the framework of a research program of Hubert Curien Tassili (PHC). Our thanks therefore go first of all to the various actors involved in the implementation of this project. The authors are grateful for the support of the Algerian Ministry of Higher Education and Scientific Research (MESRS), the General Directorate of Scientific Research and Technological Development (DGRSDT) of Algeria, the University of Tlemcen/Algeria, the CNRS and the University of Lille/France.

**Conflicts of Interest:** The authors declare that they have no known competing financial interest or personal relationships that could have appeared to influence the work reported in this paper.

## References

1. Zhao, C.; Hu, Y.; Xu, J.; Yu, M.; Zou, C.; Wang, Q.; Gao, Y.; Yang, H. Research on the Morphology, Electro-Optical Properties and Mechanical Properties of Electrochromic Polymer-Dispersed Liquid Crystalline Films Doped with Anthraquinone Dyes. *Crystals* **2023**, *13*, 735. [[CrossRef](#)]
2. Islam, M.S.; Chan, K.-Y.; Thien, G.S.H.; Low, P.-L.; Lee, C.-L.; Wong, S.K.; Noor, E.E.M.; Au, B.W.-C.; Ng, Z.-N. Performances of Polymer-Dispersed Liquid Crystal Films for Smart Glass Applications. *Polymers* **2023**, *15*, 3420. [[CrossRef](#)] [[PubMed](#)]
3. Lin, H.; Zhang, S.; Saeed, M.H.; Zhou, L.; Gao, H.; Huang, J.; Zhang, L.; Yang, H.; Xiao, J.; Gao, Y. Effects of the methacrylate monomers with different end groups on the morphologies, electro-optical and mechanical properties of polymer dispersed liquid crystals composite films. *Liq. Cryst.* **2021**, *48*, 722–734. [[CrossRef](#)]
4. Hemaida, A.; Ghosh, A.; Sundaram, S.; Mallick, T.K. Evaluation of thermal performance for a smart switchable adaptive polymer dispersed liquid crystal (PDLC) glazing. *Sol. Energy* **2020**, *195*, 185–193. [[CrossRef](#)]
5. Saeed, M.H.; Zhang, S.; Cao, Y.; Zhou, L.; Hu, J.; Muhammad, I.; Xiao, J.; Zhang, L.; Yang, H. Recent Advances in The Polymer Dispersed Liquid Crystal Composite and Its Applications. *Molecules* **2020**, *25*, 5510. [[CrossRef](#)]
6. Zhou, L.; Chen, G.; Shen, W.; Zhang, C.; Lanying, Z. Effect of functionality of thiol on the optical properties of liquid crystals/polymer composite films. *Liq. Cryst.* **2021**, *48*, 313–321. [[CrossRef](#)]
7. Zhang, S.; Li, C.; Wang, Q.; Zhou, L.; Saeed, M.H.; Wang, X.; Zhang, L.; Yang, Z.; Yang, H. Fluorescence enhancement and encapsulation of quantum dots via a novel crosslinked vinyl-ether liquid crystals/polymer composite film. *Polymer* **2020**, *207*, 122834. [[CrossRef](#)]
8. Jiang, J.; McGraw, G.; Ma, R.; Brown, J.; Yang, D.-K. Selective scattering polymer dispersed liquid crystal film for light enhancement of organic light emitting diode. *Opt. Express* **2017**, *25*, 3327–3335. [[CrossRef](#)]
9. Seo, J.; Nam, S.; Jeong, J.; Lee, C.; Kim, H.; Kim, Y. Liquid Crystal-Gated-Organic Field-Effect Transistors with In-Plane Drain-Source-Gate Electrode Structure. *ACS Appl. Mater. Interfaces* **2015**, *7*, 504–510. [[CrossRef](#)]
10. Labeeb, A.M.; Ibrahim, S.A.; Ward, A.A.; Abd-El-Messieh, S.L. Polymer/liquid crystal nanocomposites for energy storage applications. *Polym. Eng. Sci.* **2020**, *60*, 2529–2540. [[CrossRef](#)]
11. Nasir, N.; Hong, H.; Rehman, M.A.; Kumar, S.; Seo, Y. Polymer-dispersed liquid-crystal-based switchable glazing fabricated via vacuum glass coupling. *RSC Adv.* **2020**, *10*, 32225–32231. [[CrossRef](#)] [[PubMed](#)]

12. Shin, S.M.; Song, J.K.; Kim, S.H. Thermal decomposition behavior and reliability evaluation of thermotropic liquid crystalline polymers. *Macromol. Res.* **2009**, *17*, 149–155. [\[CrossRef\]](#)
13. Wadhvani, R.; Sutherland, D.; Moinuddin, K.A.M.; Joseph, P. Kinetics of pyrolysis of litter materials from pine and eucalyptus forests. *J. Therm. Anal. Calorim.* **2017**, *130*, 2035–2046. [\[CrossRef\]](#)
14. Li, X.G. Thermogravimetric kinetics of thermotropic copolyesters containing p-oxybenzoate unit by multiple heating-rate methods. *J. Appl. Polym. Sci.* **1999**, *74*, 2016–2028. [\[CrossRef\]](#)
15. Alashmawy, M.M.; Hassan, H.S.; Ookawara, S.A.; Elwardany, A.E. Thermal decomposition characteristics and study of the reaction kinetics of tea-waste. *Biomass Convers. Biorefinery* **2023**, *13*, 9487–9505. [\[CrossRef\]](#)
16. Bondarchuk, I.; Bondarchuk, S.; Vorozhtsov, A.; Zhukov, A. Advanced Fitting Method for the Kinetic Analysis of Thermogravimetric Data. *Molecules* **2023**, *28*, 424. [\[CrossRef\]](#)
17. Emiola-Sadiq, T.; Zhang, L.; Dalai, A.K. Thermal and Kinetic Studies on Biomass Degradation *via* Thermogravimetric Analysis: A Combination of Model-Fitting and Model-Free Approach. *ACS Omega* **2021**, *6*, 22233–22247. [\[CrossRef\]](#)
18. Vyazovkin, S.; Linert, W. Kinetic analysis of reversible thermal decomposition of solids. *Int. J. Chem. Kinet.* **1995**, *27*, 73–84. [\[CrossRef\]](#)
19. Vyazovkin, S. Computational aspects of kinetic analysis: Part C. The ICTAC Kinetics Project—The light at the end of the tunnel? *Thermochim. Acta* **2000**, *355*, 155–163. [\[CrossRef\]](#)
20. Vyazovkin, S.; Wight, C.A. Ammonium Dinitramide: Kinetics and Mechanism of Thermal Decomposition. *J. Phys. Chem. A* **1997**, *101*, 5653–5658. [\[CrossRef\]](#)
21. Vyazovkin, S. A Unified Approach to Nonisothermal Data. *Chem. Kinet.* **1996**, *28*, 95–101. [\[CrossRef\]](#)
22. Wanjun, T.; Donghua, C. An integral method to determine variation in activation energy with extent of conversion. *Thermochim. Acta* **2005**, *433*, 72–76. [\[CrossRef\]](#)
23. Budruga, P.; Segal, E. On the Li and Tang's isoconversional method for kinetic analysis of solid-state reactions from thermoanalytical data. *J. Mater. Sci.* **2001**, *36*, 2707–2710. [\[CrossRef\]](#)
24. Friedman, H.L. Kinetics of thermal degradation of char-forming plastics from thermogravimetry. Application to a phenolic plastic. *J. Polym. Sci. Part C: Polym. Symp.* **2007**, *6*, 183–195. [\[CrossRef\]](#)
25. Ozawa, T. Kinetic analysis of derivative curves in thermal analysis. *J. Therm. Anal. Calorim.* **1970**, *2*, 301–324. [\[CrossRef\]](#)
26. Smith, B.J.; Djajasmita, M. The land molluscs of the Krakatau Islands, Indonesia. *Philos. Trans. R. Soc. London. B Biol. Sci.* **1988**, *322*, 379–400. [\[CrossRef\]](#)
27. Li, C.-R.; Tang, T.B. A new method for analysing non-isothermal thermoanalytical data from solid-state reactions. *Thermochim. Acta* **1999**, *325*, 43–46. [\[CrossRef\]](#)
28. Kissinger, H.E. Reaction Kinetics in Differential Thermal Analysis. *Anal. Chem.* **1957**, *29*, 1702–1706. [\[CrossRef\]](#)
29. Denisov, E.T. Solid-phase Radical Reactions and Mechanism of Oxidation of Carbon-chain Polymers. *Russ. Chem. Rev.* **1978**, *47*, 572–586. [\[CrossRef\]](#)
30. Grassieker, N. *Thermal Stability of Polymers*; RT Conley Marcel Dekker: New York, NY, USA, 1970. [\[CrossRef\]](#)
31. Emanuel, S.L.; Buchachenko, A.L. *Chemical Physics of Polymer Degradation and Stabilization*; CRC Press: Boca Raton, FL, USA, 1987.
32. Nemphos, S.P. The Oxidative Degradation of Deuteropolystyrenes. *J. Polym. Sci.* **1957**, *25*, 173–187.
33. Conley, R.T.; Valint, P.L. Oxidative degradation of poly(ethyl acrylate). *J. Appl. Polym. Sci.* **1965**, *9*, 785–797. [\[CrossRef\]](#)
34. Steele, R.; Jacobs, H. Thermal-Oxidative Degradation of Poly(ethyl Acrylate). *J. Appl. Polym. Sci.* **1959**, *2*, 86–92. [\[CrossRef\]](#)
35. Hu, Y.-H.; Chen, C.-Y.; Wang, C.-C. Thermal degradation kinetics of poly(n-butyl acrylate) initiated by lactams and thiols. *Polym. Degrad. Stab.* **2004**, *84*, 505–514. [\[CrossRef\]](#)
36. Li, Q.; Wang, Y.; Fan, M.; Zhang, J.; Cheng, J. Thermal degradation kinetics of poly(acrylate/ $\alpha$ -methyl styrene) copolymers. *Polym. Degrad. Stab.* **2016**, *128*, 158–164. [\[CrossRef\]](#)
37. Ors, J.; La Perriere, D. Thermogravimetric profile of decomposition of acrylate systems based on bornyl acrylate monomers. *Polymer* **1986**, *27*, 1999–2002. [\[CrossRef\]](#)
38. Matsumoto, A.; Mizuta, K.; Otsu, T. Synthesis and thermal properties of poly(cycloalkyl methacrylate)s bearing bridged- and fused-ring structures. *J. Polym. Sci. Part A Polym. Chem.* **1993**, *31*, 2531–2539. [\[CrossRef\]](#)
39. Han, X.G.; Wei, X.Y.; Wang, X.Y.; Shanks, R.A. Characterization and Thermal Behaviour of Polymer-Dispersed Liquid Crystals. *Adv. Mater. Res.* **2011**, *152–153*, 284–287. [\[CrossRef\]](#)
40. Rusen, E.; Diacon, A.; Mitran, R.-A.; Dinescu, A.; Nistor, C.; Șomoghi, R.; Boscornea, A.C.; Mănăilă-Maximean, D. E7 nematic liquid crystal encapsulated in a polymeric photonic crystal. *Eur. Polym. J.* **2022**, *175*, 111374. [\[CrossRef\]](#)
41. Selevou, A.; Papamokos, G.; Yildirim, T.; Duran, H.; Steinhart, M.; Floudas, G. Eutectic liquid crystal mixture E7 in nanoporous alumina. Effects of confinement on the thermal and concentration fluctuations. *RSC Adv.* **2019**, *9*, 37846–37857. [\[CrossRef\]](#)
42. Vlad-Bubulac, T.; Serbezeanu, D.; Hamciuc, C.; Petreus, O.; Carja, I.; Lisa, G. Preparation and Phase Behavior of Blends of Polysulfone-Based Polymers with Phosphorous-Containing Smectic-A Liquid Crystals. *Polym. Eng. Sci.* **2013**, *53*, 1209–1216. [\[CrossRef\]](#)
43. Merah, D.; Bedjaoui, L.; Zeggai, N.; Boubberka, Z.; Sarazin, J.; Boutalbi, D.; Barrera, A.; Boughrara, H.; Dubois, F.; Cazaux, F.; et al. Enhanced thermal stability of biobased crosslinked poly(isobornylacrylate-co-2-ethylhexylacrylate) copolymers. *J. Polym. Res.* **2022**, *29*, 1–11. [\[CrossRef\]](#)

44. Haloi, D.J.; Singha, N.K. Synthesis of poly(2-ethylhexyl acrylate)/clay nanocomposite by *in situ* living radical polymerization. *J. Polym. Sci. Part A Polym. Chem.* **2011**, *49*, 1564–1571. [[CrossRef](#)]
45. JSolorzano, J.A.P.; Moinuddin, K.A.M.; Tretsiakova-McNally, S.; Joseph, P. A Study of the Thermal Degradation and Combustion Characteristics of Some Materials Commonly Used in the Construction Sector. *Polymers* **2019**, *11*, 1833. [[CrossRef](#)]
46. Li, K.; Jiang, H.; Cheng, M.; Li, Y.; Yin, Z.; Luo, D.; Sun, X.W.; Liu, Y.J. Controlling morphological and electro-optical properties via the phase separation in polymer/liquid-crystal composite materials. *Liq. Cryst.* **2020**, *47*, 238–247. [[CrossRef](#)]
47. Bouriche, A.; Alachaher, L.B.; Maschke, U. Phase behaviour and electro-optical response of systems composed of nematic liquid crystals and poly (2-ethylhexylacrylate). *Liq. Cryst.* **2018**, *45*, 656–665. [[CrossRef](#)]
48. Li, J.; Wen, C.-H.; Gauza, S.; Lu, R.; Wu, S.-T. Refractive Indices of Liquid Crystals for Display Applications. *J. Disp. Technol.* **2005**, *1*, 51–61. [[CrossRef](#)]
49. Dhyani, V.; Kumar, J.; Bhaskar, T. Thermal decomposition kinetics of sorghum straw via thermogravimetric analysis. *Bioresour. Technol.* **2017**, *245*, 1122–1129. [[CrossRef](#)]
50. Gai, C.; Zhang, Y.; Chen, W.-T.; Zhang, P.; Dong, Y. Thermogravimetric and kinetic analysis of thermal decomposition characteristics of low-lipid microalgae. *Bioresour. Technol.* **2013**, *150*, 139–148. [[CrossRef](#)]
51. Tang, W.; Liu, Y.; Zhang, H.; Wang, C. New approximate formula for Arrhenius temperature integral. *Thermochim. Acta* **2003**, *408*, 39–43. [[CrossRef](#)]
52. Rathore, N.S.; Pawar, A.; Panwar, N.L. Kinetic analysis and thermal degradation study on wheat straw and its biochar from vacuum pyrolysis under non-isothermal condition. *Biomass Convers. Biorefinery* **2021**, *13*, 7547–7559. [[CrossRef](#)]
53. Chen, T.-J.; Lin, G.-J.; Chen, B.-Y.; Lin, B.-R.; Wu, J.-J.; Yang, Y.-J. Optimized electro-optical properties of polymer-stabilized vertical-aligned liquid crystal displays driven by an in-plane field. *Displays* **2015**, *37*, 94–99. [[CrossRef](#)]
54. Doyle, C.D. Estimating isothermal life from thermogravimetric data. *J. Appl. Polym. Sci.* **1962**, *6*, 639–642. [[CrossRef](#)]
55. Varma, A.K.; Lal, N.; Rathore, A.K.; Katiyar, R.; Thakur, L.S.; Shankar, R.; Mondal, P. Thermal, kinetic and thermodynamic study for co-pyrolysis of pine needles and styrofoam using thermogravimetric analysis. *Energy* **2021**, *218*, 119404. [[CrossRef](#)]
56. Kissinger, H.E. Variation of peak temperature with heating rate in differential thermal analysis. *J. Res. Natl. Bur. Stand.* **1956**, *57*, 217. [[CrossRef](#)]
57. Starink, M.J. Activation energy determination for linear heating experiments: Deviations due to neglecting the low temperature end of the temperature integral. *J. Mater. Sci.* **2007**, *42*, 483–489. [[CrossRef](#)]
58. Krongauz, V.V. Crosslink density dependence of polymer degradation kinetics: Photocrosslinked acrylates. *Thermochim. Acta* **2010**, *503–504*, 70–84. [[CrossRef](#)]
59. Sun, J.; Huang, Y.; Gong, G.; Cao, H. Thermal degradation kinetics of poly(methylphenylsiloxane) containing methacryloyl groups. *Polym. Degrad. Stab.* **2006**, *91*, 339–346. [[CrossRef](#)]
60. Grassie, N.; Speakman, G. Thermal Degradation of Poly(alkyl Acrylates). I. Preliminary Investigations. *J. Polym. Sci. Part A-1 Polym. Chem.* **1971**, *9*, 919–929. [[CrossRef](#)]
61. Aliev, F.; Zgonnik, V. Thermo-optics and thermal stability of poly(alkyl methacrylates) in porous matrices. *Eur. Polym. J.* **1991**, *27*, 969–973. [[CrossRef](#)]
62. Zhang, L.; Zhu, Y.; Yin, W.; Guo, B.; Rao, F.; Ku, J. Isothermal Coal-Based Reduction Kinetics of Fayalite in Copper Slag. *ACS Omega* **2020**, *5*, 8605–8612. [[CrossRef](#)]
63. Yao, Z.; Yu, S.; Su, W.; Wu, W.; Tang, J.; Qi, W. Kinetic studies on the pyrolysis of plastic waste using a combination of model-fitting and model-free methods. *Waste Manag. Res. J. Sustain. Circ. Econ.* **2020**, *38*, 77–85. [[CrossRef](#)] [[PubMed](#)]

**Disclaimer/Publisher’s Note:** The statements, opinions and data contained in all publications are solely those of the individual author(s) and contributor(s) and not of MDPI and/or the editor(s). MDPI and/or the editor(s) disclaim responsibility for any injury to people or property resulting from any ideas, methods, instructions or products referred to in the content.